The Cryosphere Discuss., 9, 2915–2953, 2015
www.the-cryosphere-discuss.net/9/2915/2015/
doi:10.5194/tcd-9-2915-2015

The Cryosphere Discussions
Open Access

The relative contributions of calving and surface ablation to ice loss at a lake-terminating glacier

M. Chernos[1], **M. Koppes**[1], **and R. D. Moore**[1,2]

[1]Department of Geography, University of British Columbia, 1984 West Mall, Vancouver, BC, V6T 1Z2, Canada
[2]Department of Forest Resources Management, Forest Sciences Centre, 2424 Main Mall, Vancouver, BC, V6T 1Z4, Canada

Received: 20 April 2015 – Accepted: 27 April 2015 – Published: 27 May 2015

Correspondence to: M. Chernos (mchernos@gmail.com)

Published by Copernicus Publications on behalf of the European Geosciences Union.

Abstract

Bridge Glacier is a lake-terminating glacier in the Coast Mountains of British Columbia and has retreated over 3.55 km since 1972, with the majority of the retreat having occurred since 1991. This retreat is out of proportion to surface melt inferred from regional climate indices, suggesting that it has been driven primarily by calving as the glacier retreated across an over-deepened basin. In order to better understand the primary drivers of mass balance, the relative importance of surface melt and calving is investigated during the 2013 melt season using a distributed energy balance model and time-lapse imagery. Calving is responsible for 23 % of the mass loss during the 2013 melt season, and is limited by modest flow speeds and a small terminus cross-section. Calving and summer balance estimates over the last 30 years suggest that calving is consistently a smaller contributor of mass loss relative to surface melt. Although calving is estimated to be responsible for up to 49 % of ice loss for individual seasons, averaged over multiple summers it typically accounts for 10 to 25 %. Calving has been driven primarily by buoyancy and water depths, and fluxes were greatest between 2005 and 2010 as the glacier retreated over the deepest part of Bridge Lake. These losses are part of a transient stage in the glacier's retreat, and are expected to diminish as the terminus recedes into shallower water. Surface melt is the primary driver of ice loss at Bridge Glacier, and future mass loss and retreat is dependent on governing climatic conditions.

1 Introduction

Since the end of the Little Ice Age, glaciers across the globe have been shrinking at an accelerated rate (e.g. Dyurgerov et al., 2002; Dyurgerov and Meier, 2005). Although this retreat has been irregular, a general trend of 20th century retreat is pervasive, and well correlated with an increase in global mean temperatures (Oerlemans, 2005). The reduction in ice cover in mountainous regions has raised concern about potential changes in the timing, volume, and duration of summer streamflow (e.g. Marshall et al., 2011; Stahl et al., 2008). These changes have major implications for hydroelectric projects, agriculture, aquatic habitat, water quality, and eustatic sea level rise (Barry, 2006). While recent glacier retreat is well documented (e.g. Kaser et al., 2006), the projection of future retreat is critical to the management of water resources and understanding the evolution of riparian and aquatic habitats (Milner and Bailey, 1989; Cowie et al., 2014).

Due to their sensitivity to air temperatures and precipitation, glaciers serve as important high altitude climate stations (Oerlemans, 2005; Kaser et al., 2006). However, glaciers that terminate in bodies of water have been shown to respond at least partially independent of climate on decadal timescales (Warren and Kirkbride, 2003; Post et al., 2011). This blurring of the climate-glacier signal is due to calving, which can be an important additional source of ice loss (Benn et al., 2007a). While the climatic signal from a calving glacier is more complex than one from glaciers that terminate on land (Van der Veen, 2002; Motyka et al., 2003), their inherent instability suggests that they have the potential to contribute disproportionately to eustatic sea level rise (Meier and Post, 1987; Dyurgerov and Meier, 2005), highlighting their important role in glacier response to climate.

Although understanding the dynamics of lake-terminating glaciers is of critical importance for better watershed management and for unravelling the climatic signal in calving glaciers, few lake-calving glaciers have been studied worldwide. Work exploring the dynamics of lake-calving glacier systems has focused on Mendenhall Glacier in Alaska (Motyka et al., 2003; Boyce et al., 2007), Tasman Glacier in New Zealand (Warren and Kirkbride, 2003; Dykes et al., 2011; Dykes and Brook, 2010), and Perito Mereno Glacier in Patagonia (Warren and Sugden, 1993; Warren and Aniya, 1999; Stuefer et al., 2007). Here we present new data from Bridge Glacier, a lake-terminating outlet glacier of the Lillooet Icefield in the Coast Mountains of British Columbia, Canada. Bridge Glacier presents another valuable study site to supplement this worldwide database.

TCD
9, 2915–2953, 2015

Few studies have compared mass losses from calving and surface ablation in order to assess the relative importance of calving on the mass balance of a lake-terminating glacier. A better understanding of the glaciological, lacustrine, and climatological conditions related to calving is needed to assess the drivers that promote ice loss. Furthermore, these data will help elucidate the broad commonalities between calving glaciers worldwide, allowing for a more universal understanding of calving in freshwater glacier-lake systems.

This study investigates the relative importance of current and historical calving and surface melt at lake-terminating Bridge Glacier. Ice loss from surface melt and calving are estimated for the 2013 melt season from field measurements and distributed energy balance and calving models, and are compared to calving fluxes and surface melt rates from 1984 to present. This study contextualizes calving rates from Bridge Glacier using findings from other lacustrine calving glaciers in Alaska, New Zealand and Patagonia to highlight how the relative importance of calving and surface melt change over the transient calving phase of a retreating alpine lake-terminating glacier.

2 Study area and retreat history

Bridge Glacier (50°48′11″ N, 123°38′40″ W), an outlet of the Lillooet Icefield, is located in the Pacific Ranges of the Coast Mountains of southwestern British Columbia, Canada, roughly 175 km north of Vancouver. The glacier had an area of 83 km^2 as of the end of the 2013 melt season, extending from an elevation of over 2900 m at Bridge Peak, to 1390 m, where it terminates in a proglacial lake, locally known as Bridge Lake (see Fig. 1). The lake has grown from under 2 km^2 in 1972 to over 6 km^2 in 2013 as the glacier retreated across an overdeepened basin. The glacier has experienced large tabular calving events since the early 1990s, indicative of a floating terminus. The far (east) end of the lake traps numerous large (several hundred m^2) icebergs which are pressed along a submerged terminal moraine by persistent katabatic winds, and have been present, in most cases, for several years.

Bridge Glacier lies on the divide between the humid coastal Pacific Ranges and the drier interior Chilcotin Ranges. Synoptic air flow is predominantly from the west, generating heavy snowfall on the highest elevation, most westerly areas, while the eastern flank of the glacier is drier, with a mean May 1 SWE of 600 mm (BC Ministry of Environment, 2014).

The annual retreat of Bridge Glacier, derived from delineations of the terminus using repeat Landsat imagery since 1972 (Fig. 2), is comprised of several stages. Retreat was slow prior to 1991, characterized by small calving events along the shallow proglacial lake margin. The average rate of retreat between 1972 and 1991 was $21\,\mathrm{m\,a^{-1}}$, but accelerated to $144\,\mathrm{m\,a^{-1}}$ after 1991, punctuated by high annual retreat rates followed by years of relative terminus stability, and the appearance of large tabular icebergs in the lake. The rate of retreat accelerated again after 2009 to $\sim 400\,\mathrm{m\,a^{-1}}$ (Fig. 3e).

The substantial retreat that Bridge Glacier has undergone since 1991 cannot be fully explained by regional climate indicies (Fig. 3). For instance, from 1988 to 1998, summer temperatures, equilibrium line altitudes, and discharge from Bridge Lake were all above the 30 year average (Fig. 3a–d), suggesting above average melting of the glacier surface. This period of elevated conditions for melt did not continue into the 21st century, however, retreat continued to accelerate. Since the mid-1990s, it appears that retreat was decoupled from climate. While it is clear the acceleration of retreat as of 1991 is largely due to accelerated rates of calving, it remains unclear to what extent calving contributed to the total volume of ice loss from Bridge Glacier over the past 30 years.

3 Field methods

Three automatic weather stations (AWS) collected data from 20 June to 12 September 2013, to provide input data for a distributed energy balance melt model (see Fig. 1). One weather station was installed on-glacier (Glacier AWS) and collected air temper-

TCD
9, 2915–2953, 2015

ature, humidity, wind speed and direction, and reflected shortwave radiation at 10 min intervals. A second weather station (Ridge AWS), installed on a ridge ∼ 250 m above the glacier toe and hence shielded from strong, persistent katabatic flow, collected ambient temperature and solar radiation. A third weather station, located along the shore of Bridge Lake (Lake AWS) approximately 3 km from the terminus, on a partially submerged end moraine, measured incoming longwave radiation, air temperature, humidity, wind speed, and rainfall. Rainfall was also measured at an exposed nunatak north of the main arm of the glacier (Nunatak TLC), to estimate the precipitation gradient over the glacier tongue.

In order to ground-truth surface melt derived from from melt modelling, 3 m-long ablation stakes were installed at six locations in the ablation area. Due to logistical challenges, and to obtain results that could also be used to ground-truth velocity estimates, the stakes were located within 2 km of the terminus (Fig. 1). The stakes were installed on 18 June, and resurveyed on 19 July and 13 September 2013.

The bathymetry of Bridge Lake was collected using a Lowrance HDS Gen2 depth-sounder, with a depth range of 500 m and horizontal GPS accuracy of ±5 m. Depth measurements were taken at 893 discrete points in an irregular grid. Access to the terminus and the middle part of the lake was hindered by the presence of icebergs. An additional 74 points were added by linear interpolation using known depths along east-west transects to improve coverage. The bathymetric data were processed using the gstat package in R (R Core Team, 2013; Pebesma, 2004), and interpolated onto a 10 m grid using inverse distance weighting.

The change in terminus area during the study period was computed from Landsat images on 23 June and 11 September 2013. Shapefiles for both scenes were generated by manually delineating the terminus in Google Earth. The change in area was then calculated using the rgeos package in R.

The terminus flow velocity was measured by tracking features from two time-lapse cameras (at Nunatak TLC, and 1.5 km east) set up to capture the floating terminus and the glacier surface roughly 1 km up-glacier. Points were tracked manually using Tracker video analysis and modelling tool (Brown, 2014). Raw pixel displacement was converted into distances using known camera angles and several ground control points. Eight points in close proximity on the glacier surface (< 200 m) were tracked from each camera throughout the study period using daily noon-time images. Filtering routines discarded roughly 10 % of the tracked data points due to negative displacement, or loss of target. Daily surface velocities were generated by averaging the daily displacements for each tracked point, and the average summer velocity was calculated by averaging the total displacement for each tracked point throughout the study period. Study-period time-lapse velocity measurements were complemented with an end-of-summer survey of ablation stakes; results were found to agree within the error of our Garmin eTrex GPS (±5 m).

4 Modelling surface melt

Elevation data for the glacier surface were obtained using a 25 m resolution LIDAR digital elevation model (from C-CLEAR by M. Demuth, C. Hopkinson, and B. Menounos, see Acknowledgements). The DEM was resampled to 50 m to reduce computation time and digital artifacts in the data. To obtain historical estimates of surface melt, annual terminus retreat and equilibrium line altitudes (ELAs) were reconstructed from satellite imagery, using Landsat images from 1984 to 2012. All Landsat data were taken from images between 12 September and 24 October to represent end-of-season snowlines.

The volume of ice lost by surface melt during the 2013 summer season was computed with a distributed energy balance model using the data from the three AWS and the digital elevation model of the glacier surface. Surface melt of ice (M), in m (w.e.) d^{-1}, was calculated as

$$M = \frac{Q_M}{L_f \rho_i} \tag{1}$$

TCD
9, 2915–2953, 2015

where Q_M is the sum of available energy at the surface ($W\,m^{-2}$), L_f is the latent heat of fusion ($3.34 \times 10^6\,J\,kg^{-1}$), and ρ_i is the density of ice ($917\,kg\,m^{-3}$). Energy supplied to the glacier surface is positive, while energy flux away from the surface is negative. The available energy for melt was calculated as

$$Q_M = Q^* + Q_H + Q_E + Q_R \tag{2}$$

where Q^* is the net radiation, Q_H and Q_E are the sensible and latent heat flux, and Q_R is sensible heat of rain. All energy fluxes are in $W\,m^{-2}$. We assume that all energy fluxes occur at the ice surface (Oerlemans, 2010; Munro, 2006); subsurface and subglacial melt is neglected.

4.1 Snowline retreat

As our purpose was to calculate the total ice loss during the melt season only, we only consider ice melt and not snowmelt, and hence the model was only applied to the glacier surface below the snowline at each time step. In order to calculate the volume of ice melt at each time step, snowline retreat over the course of the summer melt season was reconstructed from nine Landsat images obtained from the LandsatLook Viewer (U. S. Geological Survey, 2014) between 1 June and 19 September 2013. Multiple measurements of snowline altitude across the glacier surface were taken for each image, and averaged to produce a basin-wide snowline elevation. Temporal interpolation between snowline elevations was achieved using the loess smoothing function in R. The snowline was at the terminus until 15 June, and the ablation area had become snow-covered again before 20 September, suggesting our field instrumentation captured all but 12–15 days of melt in the 2013 season. We estimate that ice loss during this period is less than 10 % of the total surface ice loss during the study period.

4.2 Net radiation

Net radiation (Q^*) is calculated as the sum of incoming (↓) and outgoing (↑) shortwave and longwave (L) radiation as follows:

$$Q^* = (S\downarrow + D\downarrow)(1-\alpha) + (L\downarrow - L\uparrow) \tag{3}$$

where shortwave radiation (K) is separated into direct (S) and diffuse (D) components, and α is the albedo of ice.

Reflected shortwave radiation was measured on-glacier and on bare ice in the ablation area, throughout the melt season. Incoming shortwave radiation was measured from the off-glacier Ridge AWS. Differences in shading between the two sites were found to be negligible. To minimize the effects of small discrepancies in shading, uneven cloud patterns, and low solar angle errors (Oerlemans, 2010), the daily ice albedo (α) is assumed constant throughout the day, and is calculated as

$$\alpha = \int K\uparrow \mathrm{d}t \Big/ \int K\downarrow \mathrm{d}t \tag{4}$$

where the integrals are over the period of daylight each day.

Direct shortwave radiation ($\mathrm{W\,m^{-2}}$) for each gridpoint on the glacier surface is calculated as

$$S\downarrow_{i,j} = S\downarrow \frac{K_{\mathrm{ex}_{i,j}}}{K_{\mathrm{ex}}} \tag{5}$$

where $K_{\mathrm{ex}_{i,j}}$ is the potential direct solar radiation at grid point (i,j) and K_{ex} is the potential direct solar radiation at Glacier AWS. Measured global radiation was separated into direct and diffuse components based on the ratio of observed to potential shortwave radiation following Collares-Pereira and Rabl (1979) and Hock and Holmgren (2005). Potential direct radiation was corrected for slope geometry and diffuse shortwave radiation is calculated for all cells when $K_{\mathrm{ex}} > 0$ (Hock and Holmgren, 2005; MacDougall

TCD
9, 2915–2953, 2015

and Flowers, 2011) as

$$D_{i,j} = D_{\mathrm{o}}\phi_{i,j} + \alpha_{\mathrm{terrain}} K\downarrow(1-\phi_{i,j}) \tag{6}$$

where D_{o} is the global diffuse radiation, corrected using the sky view factor (ϕ) for each grid cell.

Due to the complications and heterogeneity involved in measuring the albedo for the surrounding non-glaciated terrain ($\alpha_{\mathrm{terrain}}$), a constant value of 0.17 was assumed, which is within the range for dark, rocky surfaces (Oke, 1988). Sky view factor was calculated using SAGA GIS software and a 25 m lidar DEM. The algorithm integrates the maximum horizon angles (H) for each grid cell, for each azimuth angle (1° interval). A maximum 10 km × 10 km search window was implemented to reduce computation time.

In order to spatially distribute incoming shortwave radiation, each grid point is modelled as either shaded or sunlit. A shading algorithm was implemented that calculates the maximum horizon angle for each grid point within a 10 km × 10 km window, using 10° azimuth bins. At each time step, if the horizon angle is greater than the elevation angle (Z), the grid point is shaded, and only receives diffuse radiation. For times when the horizon angle is smaller than elevation angle, the grid point receives both direct and diffuse radiation.

Incoming longwave radiation was measured directly at the Lake AWS. In order to distribute longwave radiation across the glacier, it is scaled by the sky view factor (ϕ) as

$$L\downarrow_{i,j} = L\downarrow_{\mathrm{aws}}\frac{\phi_{i,j}}{\phi_{\mathrm{aws}}} + L_{\mathrm{terrain}}(1-\phi_{i,j}) \tag{7}$$

where additional longwave input is supplied by the surrounding terrain (L_{terrain}). Terrain temperature is assumed to equal air temperature, and the Stefan–Boltzmann equation is used with an emissivity ($\varepsilon_{\mathrm{terrain}}$) of 0.95 and an ice emissivity (ε) of 0.98 (Oke, 1988).

TCD
9, 2915–2953, 2015

4.3 Turbulent heat fluxes

Sensible and latent heat fluxes are calculated using the bulk transfer approach:

$$Q_H = \rho_{air} c_a C u (T_g - T_s) \tag{8}$$

$$Q_E = \rho_{air} L_v C u \left(\frac{0.622(e_g - e_s)}{P} \right) \tag{9}$$

where c_{air} is the specific heat capacity of air (1006 J kg^{-1} K^{-1}), u is the windspeed (m s^{-1}), T_g is the on-glacier air temperature, T_s is the glacier surface temperature (held constant at 273.15 K), L_v is the latent heat of vaporization (2.50 $\times 10^6$ J kg^{-1}), e_g and e_s are the vapour pressures (hPa) of air and glacier surface (held constant at 6.11 hPa, assuming the glacier surface is at the melting point), and P is the atmospheric pressure (hPa) at Glacier AWS. The turbulent transfer coefficient C (unitless) is calculated using bulk Richardson Numbers, using a roughness length for momentum of 2.5 mm for ice (Munro, 1989), and calculating the roughness length for temperature and vapour following Hock (1998).

Air temperature was distributed over the glacier surface using the approach developed by Shea and Moore (2010), which accounts for the effects of katabatic flow. In this approach, the magnitude of katabatic forcing was modelled as a function of the temperature difference (ΔT) between the on-glacier Glacier AWS (T_g) and off-glacier Ridge AWS (T_a, outside the katabatic boundary layer). Temperature differences were separated into upslope (northeasterly) and downslope katabatic (southwesterly) flows, based on the wind directions of Glacier AWS. Linear regression against off-glacier temperature (T_a, Fig. 4) shows a positive linear increase in ΔT, indicating the magnitude of katabatic forcing increases with increasing off-glacier air temperatures. Conversely, ΔT does not significantly vary as a function of off-glacier temperatures during upslope flow, although temperatures above 10 °C during these episodes were rare. The elevations of

TCD
9, 2915–2953, 2015
The relative contributions of calving and surface ablation
M. Chernos et al.

both weather stations are within 100 m, and small corrections to potential temperature using a $-6\,^{\circ}\mathrm{C\,km^{-1}}$ lapse rate did not produce a meaningful difference in the linear fit.

On-glacier air temperature for each grid point is modelled as a function of the katabatic temperature depression where

$$T_{\mathrm{g}} = T_{\mathrm{a}} - (k_1 T_{\mathrm{a}} + \Delta T^*) \tag{10}$$

and ΔT^* is the threshold temperature differential at which katabatic flow is observed. The magnitude of katabatic forcing for each point on the glacier, k_1, is calculated using statistical coefficients and glacier flow path lengths (Shea, 2010; Chernos, 2014). Flow path lengths for the glacier were calculated using the Terrain Analysis – Hydrology module of SAGA GIS (Quinn et al., 1991; SAGA Development Team, 2008). During periods when wind direction is upslope, temperatures are distributed using the on-glacier temperature, T_{g}, and a standard temperature lapse rate of $-6\,^{\circ}\mathrm{C\,km^{-1}}$.

Wind speed across the glacier was distributed as a function of katabatic forcing and ambient temperatures, following Shea (2010). For situations when the measured on-glacier wind direction was downslope, wind speed increases linearly with increasing off-glacier air temperature, while upslope wind speeds show no significant change. When the measured on-glacier wind direction is upslope, wind speed is held constant, using measured wind speeds from Glacier AWS.

Vapour pressure is calculated from measured relative humidity and saturation vapour pressure (e_{sat}). Relative humidity, measured at Glacier AWS, is held spatially constant across the glacier for each timestep, and saturation vapour pressure is calculated from distributed on-glacier air temperatures.

4.4 Melt contribution from rain

Energy supplied to the surface due to rain was calculated as

$$Q_{\mathrm{R}} = \rho_{\mathrm{w}} c_{\mathrm{w}} R T_{\mathrm{R}} \tag{11}$$

TCD
9, 2915–2953, 2015

where R is the rainfall rate ($\mathrm{m\,s^{-1}}$), measured at the Lake AWS (and missing values are filled with measured data from Nunatak TLC), and ρ_w and c_w are the density ($1000\,\mathrm{kg\,m^{-3}}$) and specific heat of water ($4180\,\mathrm{J\,kg^{-1}\,K^{-1}}$). The temperature of rain, T_R, is assumed equal to the ambient off-glacier air temperature, and is corrected for elevation using a standard lapse rate.

5 Modelling calving flux

Calving losses are calculated from measured retreat rates and flow speeds, as well as estimates of ice thickness derived from bathymetry. The volume of ice discharged through calving from the glacier terminus, Q_calving ($\mathrm{m^3\,a^{-1}}$), i.e., the calving flux, can be quantified as

$$Q_\mathrm{calving} = \left(\frac{\mathrm{d}A_\mathrm{T}}{\mathrm{d}t} + UW\right) H_\mathrm{I} \tag{12}$$

where $\frac{dA_\mathrm{T}}{dt}$ is the change in glacier surface area at the terminus ($\mathrm{m^2\,a^{-1}}$), U is the terminus flow velocity ($\mathrm{m\,a^{-1}}$), H_I and W are the ice thickness (m) and glacier width (m) at the terminus. Subaqueous melt at the ice front is assumed to be negligible with respect to the magnitude of the calving flux.

The thickness of ice at the terminus was approximated by assuming that the terminus is floating. Using the height above buoyancy criterion (Van der Veen, 1996; Benn et al., 2007b), the ice thickness (H_I) can be calculated as

$$H_\mathrm{I} = H_\mathrm{b} + \frac{\rho_\mathrm{w}}{\rho_\mathrm{i}} D_\mathrm{W} \tag{13}$$

where H_b is the height of ice above the waterline (m), D_W is the water depth, while ρ_w and ρ_i are the densities of water and ice. The validity of this assumption is supported by the observation that large tabular icebergs that calved during the melt season showed

TCD
9, 2915–2953, 2015

Title Page
Abstract Introduction
Conclusions References
Tables Figures
◀◀ ▶▶
◀ ▶
Back Close
Full Screen / Esc
Printer-friendly Version
Interactive Discussion

limited mobility immediately after calving, suggesting that the glacier is close to the boundary criterion for flotation. There is a notable inflection point (Fig. 5), where it is assumed that the terminus transitions from grounded to floating.

The calving flux between 1984 and 2012 was computed from historical terminus positions, lake bathymetry (Fig. 6), estimated ice thickness, and measured velocity from the 2013 field season. Historical terminus velocities were assumed to be approximately equal to the 2013 summer flow speed (140 $\mathrm{m\,a^{-1}}$), and annual calving rates are calculated with 70 $\mathrm{m\,a^{-1}}$ (50 %) potential variability around the 2013 mean.

From the repeat Landsat imagery, it is clear that the terminus became ungrounded and achieved flotation around 1991. Given that terminus velocities are presumed to be a function of basal drag (Benn et al., 2007a), once the terminus achieved flotation it is likely that terminus flow speeds have not changed dramatically since then. However, we recognize that terminus velocities were likely slower when the calving front was grounded, and hence we are likely overestimating calving rates prior to 1991.

A 60 m uncertainty in measuring the terminus cross-section (W) (equal to 2 Landsat pixels) is applied. The uncertainty of $\frac{dA}{dt}$ is estimated as 7200 $\mathrm{m^2\,a^{-1}}$ (2 m × 60 m × 60 m). The ice thickness uncertainty is estimated as 5.6 % plus an additional 10 m to account for changes in sedimentation and ice thickness relative to water depth. Before 1991, the terminus was not floating; therefore, an ice thickness uncertainty of 60 m is estimated to account for a range of grounded terminus geometries. Between 1991 and 2004, bathymetry has poor data coverage, and a ice thickness uncertainty of 33 m is estimated.

6 Historical surface melt

In order to understand the long-term mass loss at Bridge Glacier, estimates of historical surface melt are derived using ELA observations and a fitted linear mass balance gradient (Shea et al., 2013). Below the snowline, the net balance (where $b_n = b_w + b_s$) is equal to the glacier ice loss, and is estimated using the 2013 glacier hypsometry, where

$$b_n(z) = b_1(\mathrm{ELA} - z) \tag{14}$$

and is calculated for the elevation of every point, z (m a.s.l.), below the ELA.

The coefficient value (b_1 = 6.62 m (w.e.) m^{-1}) taken from Shea et al. (2013) underestimates the volume of ice loss during the 2013 melt season calculated from the distributed energy balance model. Coefficient b_1 is derived from the mass balance gradient from the DEBM (9.07 m (w.e.) m^{-1}, Fig. 7), and is used for all years.

The glacier area is determined from the end-of-season calving margin. Calved area is given an elevation of 1400 m (a.s.l.) and are considered in Eq. (14). Historical ELAs are measured from end-of-summer (mid-September to mid-October) Landsat images from 1984 to 2013.

Errors in ELA-derived mass balance calculations are estimated by assuming a 75 m uncertainty in measuring the ELA, due to timing of available Landsat images, or 22 % according to Shea et al. (2013), whichever is greater. The ELA uncertainty estimate is to account for errors that cannot be adequately quantified without additional historical data, such as the linearity of the mass balance gradient.

7 Results

7.1 The 2013 surface melt

From 20 June to 12 September 2013, our model predicted 1.0 m (w.e.) of surface ice loss of near the ELA to 5.9 m (w.e.) near the terminus, yielding a total mass loss of 0.124 km^3 (Fig. 8). Melt rates are greatest along the main tongue of the glacier, due to high sensible heat flux driven by persistent katabatic flow. The southernmost tributary glacier shows relatively low melt rates relative to its elevation, most likely due to the fact that it remained sheltered from high winds and its north-facing aspect allowed for substantial shading throughout the melt season.

TCD
9, 2915–2953, 2015

Modelled melt agreed within ±0.2 m w.e. for four of the five ablation stakes (Fig. 9), representing an error of less than 5 % of the measured value. Measured melt at ablation stake D, located roughly 400 m up-glacier (∼ 100 m increase in elevation) from Glacier AWS and stake A, is up to 0.8 m less than other nearby stakes (including stake E, which is 200 m higher in elevation, and further up-glacier), suggesting that there may have been errors in measurement, or localized effects shielding the stake from higher melt rates observed elsewhere in the ablation area.

7.2 The 2013 calving flux

The terminus retreated 65 m over 85 days in 2013, with a change in terminus area of $-0.297\,\mathrm{km}^2$. The average velocity at the terminus was $139\,\mathrm{m\,a}^{-1}$, across a width of 1055 m, yielding an additional loss of $0.0342\,\mathrm{km}^2$ due to calving.

Water depth was estimated from a cross-section parallel to, and roughly 500 m from, the June 2013 terminus position. The median depth was 109 m, corresponding to a height above buoyancy of 9.9 m, and an estimated ice thickness of 109 m. Combining these measurements in Eq. (12) yields an estimated calving flux of $0.0362\,\mathrm{km}^3$ for the 85 day study period.

Comparing the volume of mass lost through calving with the volume of surface ice melt during the same period yields a total mass loss of $0.160\,\mathrm{km}^3$ of ice. For the 2013 melt season, calving accounts for 23 % of the mass loss, equivalent to an additional 1.3 m of surface melt over the entire ablation area.

7.3 Historical ice loss

The volume of ice lost from surface melt over the past 30 years was predominantly a function of the position of the ELA, and showed only a minor decrease over time. Between 1984 and 2013, the ELA varied from 1926 to 2202 m; however, in most years the ELA was between 2050 and 2150 m, resulting in a standard deviation in volumetric ice loss of $0.018\,\mathrm{km}^3$. The surface ablation in 2013 was above the 30 year average, but within one standard deviation of the mean ($\bar{x} = 0.107\,\mathrm{km}^3$). Surface melt showed a minor decrease over time, which can be attributed to the loss of surface area in the lowest reaches of the glacier due to calving and retreat.

Historical calving losses are characterized by several years of high flux, and periods of relative stability. The magnitude of the calving losses increased once the glacier achieved flotation in 1991. Calving losses are minimal before 1991, most likely due to the relative stability of a grounded terminus. From 1992 to 1994, the calving flux increased to 0.020–0.029 km^3 (19–27 % of the total annual ice loss), before a two year period of low flux (< 0.015 km^3). From 1997 to 2000, calving losses increased again (0.023–0.052 km^3), before settling into another period of relative stability in 2001–2002. The highest calving fluxes occurred between 2003 to 2006 (0.030–0.084 km^3) and again from 2008 to 2011 (0.036–0.100 km^3) with a period of stability in 2006–2007. As the calving flux increased in the period from 2003–2011, surface ablation rates decreased, resulting in the calving flux becoming a larger component of total ice loss in the 21st century. The volume of ice loss due to calving was roughly equal to the volume lost due to surface melt in 2005, 2008 and 2010 (44–49 % of total volumetric ice losses).

8 Discussion

8.1 Controls on calving

During the 2013 melt season, calving was a moderate contributor of mass loss relative to surface melt at Bridge Glacier. Calving losses in this system are controlled by glaciological and topographical controls that ultimately limit the magnitude of the calving flux. The glacier width at the calving margin was just over 1 km, which restricts the volume of ice that can reach the floating terminus, in turn limiting the size of calving events. In contrast, the ablation area in 2013 was over 27.6 km^2, allowing for surface melt processes to act over a much larger area and contribute a substantially larger volume of ice loss than possible from the calving front.

Relatively modest glacier flow speeds at the terminus also limit the volume of ice delivered to the terminus and calving. Flow velocity at Bridge Glacier is moderate due to gentle gradients in the lower reaches of the glacier, as well as relatively narrow sidewalls. A gentle surface slope reduces the gravitational stresses, while narrow valley sidewalls provide substantial lateral drag (Benn et al., 2007a; Koppes et al., 2011), both of which limit flow speeds. Near-terminus flow speeds at Bridge Glacier are one to two orders of magnitude smaller than those observed at larger tidewater calving glaciers in Patagonia and Alaska (Rivera et al., 2012; Koppes et al., 2011; Meier and Post, 1987), and reflect a more stable character and configuration, similar to lake-terminating glaciers Mendenhall and Tasman (Boyce et al., 2007; Dykes et al., 2011).

Although water depths increased substantially during the highest rates of calving in the late 2000s, we do not expect major changes in terminus velocity since the terminus achieved floatation in 1991. The 2013 mean terminus water depth was within 15 m of depths during the late 2000s, and was larger than the average water depth between 2004 and 2012. Given the relative consistency in water depths, and that the terminus is assumed to have remained floating throughout this most recent stage of retreat, we do not expect large changes in resisting stresses. Furthermore, a first order examination of thinning rates using Landsat images from the last two decades does not reveal major year to year changes, suggesting that basal shear stresses, and hence velocities, have not varied significantly during this time. However, maximum water depths peaked in the mid-2000s, meaning that is is possible that velocities could have been higher during this period (Van der Veen, 1996), making our calving fluxes underestimates. Conversely, it is likely that pre-1991 velocities were substantially smaller than what was measured in 2013. As such, it is unlikely that calving losses could equal the upper bounds of our estimate during this pre-floatation period.

The bathymetry of Bridge Lake also controls the calving flux. While we note that the terminus of Bridge Glacier is partially buoyant, flotation remains dependent on the ice

TCD
9, 2915–2953, 2015

thickness at the terminus and the water depth. Any significant thickening of the glacier, without any concurrent increase in lake level, would theoretically increase the potential volume of ice lost to calving, but would also serve to reduce the buoyancy of the terminus and allow the terminus to become grounded. Grounding would stabilize the terminus, and significantly reduce potential calving losses. In other words, any increase in terminus thickness is more likely to reduce, rather than enhance, the calving flux.

8.2 The relative importance of calving

From 1984 to 2013, the calving flux increased from an almost negligible annual yield to a flux responsible for between 20–45 % of the annual ice loss. The trend in calving flux closely follows water depth at the terminus, where the largest calving fluxes coincide with the terminus retreating into the deepest parts of Bridge Lake in 2003–2011. This relationship suggests that buoyancy is a primary driver of calving at Bridge Glacier. It also implies that the high rate of calving currently observed is unsustainable over the coming decades, and is instead part of a transient phase as the glacier continues to retreat up-valley and into shallower waters.

Although calving contributed less than one quarter of the total ice loss from Bridge Glacier during the 2013 melt season, during three of the last ten years the volume of ice loss due to calving is on par with the volume lost due to surface melt. However, large annual calving fluxes do not persist over several consecutive seasons, and are instead followed by several years of only minor calving losses, even though the terminus remained in the deepest part of the lake. The pattern of a high magnitude calving year followed by several low-flux years is consistent with the notion that glacier dynamics respond to large calving events by alleviating terminus instability and inhibiting future calving (Venteris, 1999; Benn et al., 2007b). Following a large calving event, the glacier geometry changes, and buoyant forces can be redistributed or relieved, promoting terminus stability.

The historical reconstruction of calving and surface melt losses suggests that climate is the driving factor affecting the long-term health of Bridge Glacier. Although calving has produced substantial ice losses during the last 10 years, calving fluxes in most calving systems are driven by deep water and/or high flow speeds (Warren and Aniya, 1999; Van der Veen, 2002; Benn et al., 2007b). Given the lake bathymetry, and observed flow speeds at Bridge Glacier, it is unlikely that the terminus will remain in deep water for many more years, suggesting that current calving losses are transient, and unsustainable. The primary contribution of surface melt to Bridge Glacier's mass loss suggests that the glacier's future health is more dependent on climatic conditions rather than calving losses, and surface melt is expected to become even more important as the glacier nears the end of this transient calving phase.

8.3 Bridge Glacier and other lake-calving systems

Bridge Glacier falls in the middle of a continuum of magnitude and frequency of calving in other lake-terminating glaciers worldwide (see Table 1). The calving rate for Bridge Glacier (281 $\mathrm{m\,a^{-1}}$ in 2013) is larger than that for smaller glaciers in New Zealand, such as Maug, Grey and Hooker (Warren and Kirkbride, 2003), and for Mendenhall Glacier in Alaska (Motyka et al., 2003; Boyce et al., 2007). Conversely, calving rates at the larger Patagonian glaciers Leon, Ameghino, and Upsala are up to an order of magnitude greater than what we found at Bridge (Warren and Aniya, 1999).

Bridge Glacier's calving rate is controlled by moderate water depths and flow speeds. Higher calving rates are associated with greater water depths and significantly larger terminus velocities. Large Patagonian and Icelandic glaciers have terminus velocities of up to 1810 $\mathrm{m\,a^{-1}}$ (Haresign, 2004), an order of magnitude greater than what we measured at Bridge Glacier (140 $\mathrm{m\,a^{-1}}$). Conversely, smaller calving glaciers in New Zealand terminate in shallow lakes (< 50 m) and many have low flow speeds (< 70 $\mathrm{m\,a^{-1}}$). Bridge Glacier's calving rate in 2013 (281 $\mathrm{m\,a^{-1}}$) also agrees quite well with first-order linear models relating calving to water depth (Funk and Röthlisberger, 1989). Using the revised relationship from Warren and Kirkbride (2003), the modelled calving rate for Bridge Glacier is calculated as 268 $\mathrm{m\,a^{-1}}$, i.e., within 13 $\mathrm{m\,a^{-1}}$ of the rate we observed in 2013. Our observed calving rate at Bridge falls along the linear

TCD
9, 2915–2953, 2015

spectrum of calving and water depth for lake-calving glaciers worldwide, which is an order of magnitude lower than calving rates from tidewater systems (Fig. 12).

Lake temperatures also appear to play a role in controlling the calving rate. Many Patagonian icefields terminate in large lakes where water temperatures are up to 7.6 °C (Warren and Aniya, 1999), significantly warmer than the well-mixed 1 °C water observed at Bridge Lake (Bird, 2014). This difference is most likely related to the surface area of the proglacial lakes. Bridge Lake is relatively large (6.3 km^2), but is small relative to the much larger lakes of Southern Patagonia, that are greater than 300 m deep. This depth, combined with large areas that are free of the strong cooling influence of glacier runoff and trapped icebergs, allows for these proglacial lakes to warm significantly, and promote further calving.

Bridge Glacier shares similar calving characteristics with both Tasman and Mendenhall Glaciers, both of which have undergone significant retreat as they transitioned from grounded to floating termini (Boyce et al., 2007; Dykes et al., 2011). During this transition, terminus velocities increased at Tasman from 69 to 218 $m\,a^{-1}$ (Dykes and Brook, 2010; Dykes et al., 2011), while the calving rates for both glaciers increased from 50 $m\,a^{-1}$ to between 227 and 431 $m\,a^{-1}$ (Boyce et al., 2007; Dykes et al., 2011); these rates are consistent with what we found at Bridge Glacier. For both Tasman and Mendenhall Glaciers, water depth and buoyancy also control the magnitude of calving (Boyce et al., 2007; Dykes et al., 2011; Dykes, 2013), suggesting that the majority of the ice discharged from the terminus is triggered by buoyant forces. As the multi-annual calving rate is driven primarily by water depth, unless glacier flow speeds remain high enough to continually transport ice to deeper lake waters, and maintain terminus flotation, the glacier will retreat into shallow water and regain stability.

9 Conclusions

Bridge Glacier is a lake-terminating glacier in the Coast Mountains of British Columbia that has retreated over 3.55 km since 1972, with the majority of retreat occurring after

1991. This retreat was independent of regional warming trends, and was enhanced by significant calving losses as the glacier terminus retreated into deeper waters. While calving has accelerated Bridge Glacier's retreat, estimates of surface melt and the calving flux for the 2013 melt season indicate that calving was only responsible for 23 % of the total ice loss. The contribution of calving to mass loss was limited by modest terminus flow speeds, relatively narrow side-walls in the lower glacial tongue, and lake depth at the terminus.

Estimates of calving and surface melt rates from 1984 to present suggest that calving did not contribute to significant mass loss before 1991. From 1991 to 2003 calving rates increased significantly, and the calving flux was on par with the volumetric ice loss from surface melt in 2005, 2008 and 2010. Although individual years can have large calving fluxes, multi-year averages show that calving only contributed between 10 and 25 % of the total ice loss at Bridge Glacier. Therefore, the dominant control on the mass balance of Bridge Glacier is surface melt, and future projections of glacier retreat should be closely tied to climate. The rapid calving rates observed since 2009 at Bridge Glacier are part of a transient stage in retreat as the glacier terminus passes through an overdeepened, lake-filled basin, and are not expected to remain a consistently large source of ice loss in the coming decades.

Acknowledgements. This work was supported financially by operating grants to M. Koppes and R. D. Moore from the Natural Sciences and Engineering Research Council (NSERC) and a Canada Foundation of Innovation Leaders Fund grant to M. Koppes. Assistance with field data collection was provided by Lawrence Bird, Alistair Davis, and Mélanie Ebsworth. The authors gratefully acknowledge M. Demuth, C. Hopkinson, and B. Menounos for the LiDAR data used in this study, which was collected as part of a C-CLEAR effort to develop LiDAR environmental applications, and funded in part by the Western Canadian Cryospheric Network (WCCN).

References

Barry, R. G.: The status of research on glaciers and global glacier recession: a review, Prog. Phys. Geog., 30, 285–306, doi:10.1191/0309133306pp478ra, 2006. 2917

TCD

9, 2915–2953, 2015

The relative contributions of calving and surface ablation

M. Chernos et al.

BC Ministry of Environment: Historic Snow Survey Data, available at: h9p://bcrfc.env.gov.bc.ca/data/asp/archive.htm (last access: 30 September 2014), 2014. 2919

Benn, D., Hulton, N., and Mottram, R.: "Calving laws", "sliding laws" and the stability of tidewater glaciers, Ann. Glaciol., 46, 123–130, 2007a. 2917, 2928, 2932

Benn, D., Warren, C., and Mottram, R.: Calving processes and the dynamics of calving glaciers, Earth-Sci. Rev., 82, 143–179, 2007b. 2927, 2933, 2934

Bird, L.: Hydrology and Thermal Regime of a Proglacial Lake Fed by a Calving Glacier, M.S. thesis, University of British Columbia, Vancouver, Canada, 2014. 2935

Boyce, E. S., Motyka, R. J., and Truffer, M.: Flotation and retreat of a lake-calving terminus, Mendenhall Glacier, southeast Alaska, USA, J. Glaciol., 53, 211–224, doi:10.3189/172756507782202928, 2007. 2917, 2932, 2934, 2935, 2941

Brown, D.: Tracker Video Analysis and Modeling Tool, available at: https://www.cabrillo.edu/~dbrown/tracker/ (last access: 1 February 2014), 2014. 2921

Chernos, M.: The Relative Importance of Calving and Surface Ablation at a Lacustrine Terminating Glacier, M.S. thesis, University of British Columbia, Vancouver, Canada, 2014. 2926, 2941

Collares-Pereira, M. and Rabl, A.: The average distribution of solar radiation-correlations between diffuse and hemispherical and between daily and hourly insolation values, Sol. Energy, 22, 155–164, 1979. 2923

Cowie, N. M., Moore, R. D., and Hassan, M. A.: Effects of glacial retreat on proglacial streams and riparian zones in the Coast and North Cascade Mountains, Earth Surf. Proc. Land., 39, 351–365, 2014. 2917

Dykes, R. C.: A Multi-Parameter Study of Iceberg Calving and the Retreat of Haupapa Tasman Glacier, South Island, New Zealand, Ph.D. thesis, Massey University, Palmerston North, New Zealand, 2013. 2935

Dykes, R. C. and Brook, M. S.: Terminus recession, proglacial lake expansion and 21st century calving retreat of Tasman Glacier, New Zealand, New Zeal. Geogr., 66, 203–217, doi:10.1111/j.1745-7939.2010.01177.x, 2010. 2917, 2935

Dykes, R., Brook, M., Robertson, C., and Fuller, I.: Twenty-first century calving retreat of Tasman Glacier, Southern Alps, New Zealand, Arct. Antarct. Alp. Res., 43, 1–10, doi:10.1657/1938-4246-43.1.1, 2011. 2917, 2932, 2935, 2941

Dyurgerov, M. and Meier, M.: Glaciers and the Changing Earth System: a 2004 Snapshot, Institute of Arctic and Alpine Research, University of Colorado, Boulder, CO, 2005. 2916, 2917

Dyurgerov, M., Meier, M., and Armstrong, R. L.: Glacier Mass Balance and Regime: Data of Measurements and Analysis, Institute of Arctic and Alpine Research, University of Colorado, Boulder, USA, 2002. 2916

Funk, M. and Röthlisberger, H.: Forecasting the effects of a planned reservoir which will partially flood the tongue of Unteraargletscher in Switzerland, Ann. Glaciol., 13, 76–81, 1989. 2934

Haresign, E.: Glacio-Limnological Interactions at Lake-Calving Glaciers, Ph.D. thesis, University of St. Andrews, St. Andrews, Scotland, 2004. 2934, 2941, 2953

Hock, R.: Modelling of Glacier Melt and Discharge, Ph.D. thesis, ETH Zurich, Zurich, Switzerland, 1998. 2925

Hock, R. and Holmgren, B.: A distributed surface energy-balance model for complex topography and its application to Storglaciären, Sweden, J. Glaciol., 51, 25–36, 2005. 2923

Kaser, G., Cogley, J., Dyurgerov, M., Meier, M., and Ohmura, A.: Mass balance of glaciers and ice caps: Consensus estimates for 1961–2004, Geophys. Res. Lett., 33, L19501, doi:10.1029/2006GL027511, 2006. 2917

Koppes, M., Conway, H., Rasmussen, L. A., and Chernos, M.: Deriving mass balance and calving variations from reanalysis data and sparse observations, Glaciar San Rafael, northern Patagonia, 1950–2005, The Cryosphere, 5, 791–808, doi:10.5194/tc-5-791-2011, 2011. 2932

MacDougall, A. H. and Flowers, G. E.: Spatial and temporal transferability of a distributed energy-balance glacier melt model, J. Climate, 24, 1480–1498, 2011. 2923

Marshall, S., White, E., Demuth, M., Bolch, T., Wheate, R., Menounos, B., Beedle, M., and Shea, J.: Glacier water resources on the eastern slopes of the Canadian Rocky Mountains, Can. Water Resour. J., 36, 109–134, 2011. 2917

Meier, M. and Post, A.: Fast tidewater glaciers, J. Geophys. Res., 92, 9051–9058, 1987. 2917, 2932

Milner, A. M. and Bailey, R.: Salmonid colonization of new streams in Glacier Bay National park, Alaska, Aquac. Res., 20, 179–192, 1989. 2917

Motyka, R. J., O'Neel, S., Connor, C. L., and Echelmeyer, K. A.: Twentieth century thinning of Mendenhall Glacier, Alaska, and its relationship to climate, lake calving, and glacier runoff, Global Planet. Change, 35, 93–112, doi:10.1016/S0921-8181(02)00138-8, 2003. 2917, 2934, 2941

Munro, D. S.: Surface roughness and bulk heat transfer on a glacier: comparison with eddy correlation, J. Glaciol., 35, 343–348, 1989. 2925

Munro, D. S.: Linking the weather to glacier hydrology and mass balance at Peyto Glacier, in: Peyto Glacier: One Century of Science, National Hydrology Research Institute Science Report, Otawa, Canada, 278, 135–178, 2006. 2922

Oerlemans, J.: Extracting a climate signal from 169 glacier records, Science, 308, 675–677, doi:10.1126/science.1107046, 2005. 2916, 2917

Oerlemans, J.: The Microclimate of Valley Glaciers, Igitur, Utrecht Publishing & Archiving Services, Utrecht, the Netherlands, 2010. 2922, 2923

Oke, T.: Boundary Layer Climates, Routledge, London, England, 1988. 2924

Pebesma, E. J.: Multivariable geostatistics in S: the gstat package, Comput. Geosci., 30, 683–691, 2004. 2920

Post, A., O'Neel, S., Motyka, R., and Streveler, G.: A complex relationship between calving glaciers and climate, Eos, Trans. Am. Geophys. Union, 92, 305–312, 2011. 2917

Quinn, P., Beven, K., Chevallier, P., and Planchon, O.: The prediction of hillslope flow paths for distributed hydrological modelling using digital terrain models, Hydrol. Process., 5, 59–79, 1991. 2926

R Core Team: R: a Language and Environment for Statistical Computing, R Foundation for Statistical Computing, Vienna, Austria, available at: http://www.R-project.org/ (last access: 15 April 2014), 2013. 2920

Rivera, A., Corripio, J., Bravo, C., and Cisternas, S.: Glaciar Jorge Montt (Chilean Patagonia) dynamics derived from photos obtained by fixed cameras and satellite image feature tracking, Ann. Glaciol., 53, 147–155, 2012. 2932

SAGA Development Team: System for Automated Geoscientific Analyses (SAGA GIS), Germany, available at: http://www.saga-gis.org/ (last access: 15 April 2014), 2008. 2926

Shea, J. M.: Regional-Scale Distributed Modelling of Glacier Meteorology and Melt, Southern Coast Mountains, Canada, Ph.D. thesis, University of British Columbia, Vancouver, Canada, 2010. 2926

Shea, J. M. and Moore, R. D.: Prediction of spatially distributed regional-scale fields of air temperature and vapor pressure over mountain glaciers, J. Geophys. Res., 115, D23107, doi:10.1029/2010JD014351, 2010. 2925

TCD

9, 2915–2953, 2015

Shea, J. M., Menounos, B., Moore, R. D., and Tennant, C.: An approach to derive regional snow lines and glacier mass change from MODIS imagery, western North America, The Cryosphere, 7, 667–680, doi:10.5194/tc-7-667-2013, 2013. 2928, 2929, 2948
Stahl, K., Moore, R., Shea, J., Hutchinson, D., and Cannon, A.: Coupled modelling of glacier and streamflow response to future climate scenarios, Water Resour. Res., 44, W02422, doi:10.1029/2007WR005956, 2008. 2917
Stuefer, M., Rott, H., and Skvarca, P.: Glaciar Perito Moreno, Patagonia: climate sensitivities and glacier characteristics preceding the 2003/04 and 2005/06 damming events, J. Glaciol., 53, 3–16, 2007. 2917, 2941
U.S. Geological Survey: LandsatLook Viewer, available at: http://landsatlook.usgs.gov/ (last access: 1 September 2014), 2014. 2922
Van der Veen, C.: Tidewater calving, J. Glaciol., 42, 375–385, 1996. 2927, 2932
Van der Veen, C.: Calving glaciers, Prog. Phys. Geog., 26, 96–122, 2002. 2917, 2934
Venteris, E. R.: Rapid tidewater glacier retreat: a comparison between Columbia Glacier, Alaska and Patagonian calving glaciers, Global Planet. Change, 22, 131–138, 1999. 2933
Warren, C. and Aniya, M.: The calving glaciers of southern South America, Global Planet. Change, 22, 59–77, 1999. 2917, 2934, 2935, 2941
Warren, C. and Sugden, D.: The Patagonian Icefields: a glaciological review, Arctic Alpine Res., 75, 316–331, 1993. 2917
Warren, C. R. and Kirkbride, M. P.: Calving speed and climatic sensitivity of New Zealand lake-calving glaciers, Ann. Glaciol., 36, 173–178, 2003. 2917, 2934, 2941

TCD
9, 2915–2953, 2015

Table 1. Characteristics of selected major lake-calving glaciers worldwide. D_w is the mean water depth, T_w is the mean water (depth averaged or range) temperature, U_T is the terminus averaged flow speed, and U_c is the calving rate. Citations: a: Boyce et al. (2007), b: Motyka et al. (2003), c: Warren and Kirkbride (2003), d: Dykes et al. (2011), e: Warren and Aniya (1999), f: Stuefer et al. (2007), g: Haresign (2004), h: Chernos (2014), i: this study.

Location	Year	D_w (m)	T_w (°C)	U_T (m a^{-1})	U_c (m a^{-1})	Source
Alaska						
Mendenhall	1997–2004	45–52	1–3	45–55	12–431	a, b
New Zealand						
Maud	1994–1995	15	4.3	151	88	c
Grey	1994–1995	12	4.2	52	47	c
Ruth	1994–1995	4	3.1	6	36	c
Tasman	1995	10	0.5	11	28	c
	2000–2006	50	1–10	69	78	d
	2006–2008	153	1–10	218	227	d
Patagonia						
Upsala West	1995	300		1620	2020	e
Grey	1995	165		450	355	e
Ameghino	1994	130	2.8–3.3	375	370	e
Perito Mereno	1995–2006	175	5.5–7.6	535	510	e, f
Leon	2001	65	4.5–7.0	520–1810	520–1770	g
Iceland						
Fjallsjokull	2003	75	1.5–3.0	258	582	g
Canada						
Bridge	2013	109	1.1–1.5	140	281	h, i
	1984–1990	61		70–210	30	h, i
	1991–2003	90		70–210	82 (0–351)	h, i
	2004–2012	102		70–210	237	h, i

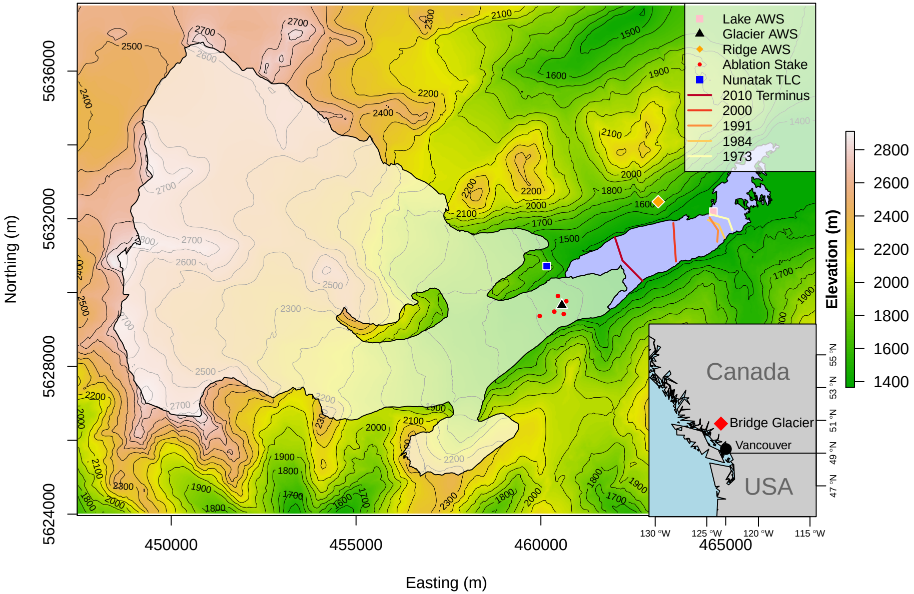

Figure 1. Bridge Glacier study area, instrumentation, and select terminus positions from 1973 to 2013. Contour intervals are 100 m.

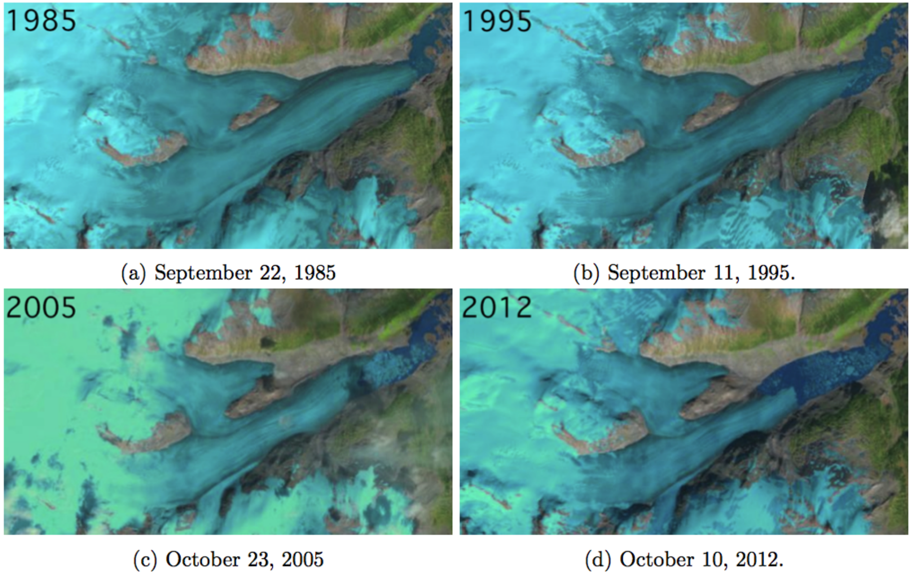

Figure 2. Landsat imagery from 1985 to 2012, showing retreat of Bridge Glacier and opening of Bridge Lake.

TCD
9, 2915–2953, 2015

The relative contributions of calving and surface ablation

M. Chernos et al.

Title Page
Abstract Introduction
Conclusions References
Tables Figures
◂ ▸
Back Close
Full Screen / Esc
Printer-friendly Version
Interactive Discussion

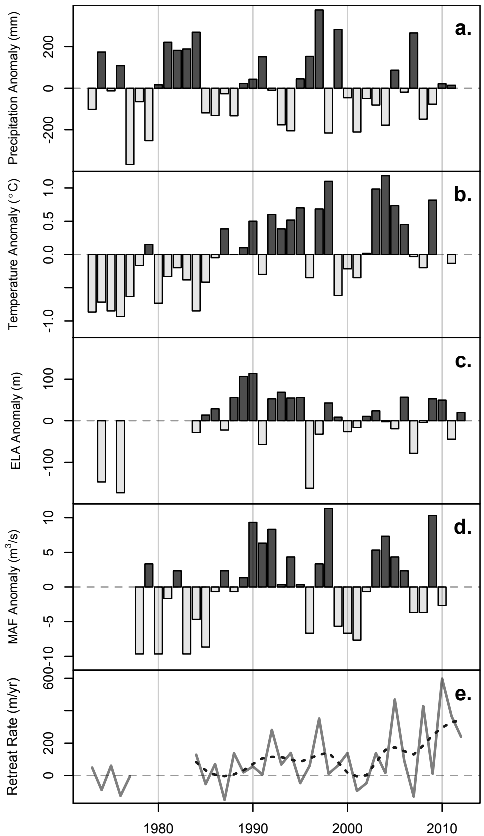

Figure 3. Summary of climatic indicators and glacier response. **(a)** Vancouver winter precipitation anomaly ($\overline{x} = 819$ mm), **(b)** Vancouver summer temperature anomaly ($\overline{x} = 14.8\,^{\circ}$C), **(c)** equilibrium line altitude ($\overline{x} = 2089$ m), **(d)** Bridge River mean annual flow anomaly ($\overline{x} = 10.7\,\mathrm{m^3\,s^{-1}}$), **(e)** Annual retreat rate ($\mathrm{m\,a^{-1}}$), dashed line is loess-smoothed retreat (span = 0.5).

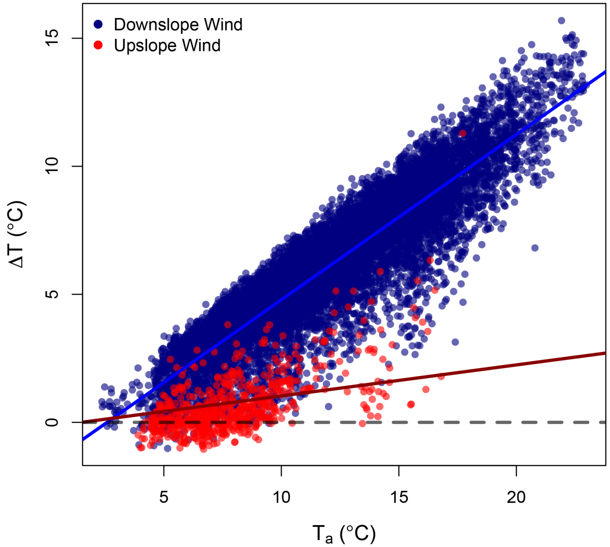

Figure 4. On glacier temperature depression ($\Delta T = T_a - T_g$) as a function of ambient air temperatures (T_a) from Ridge AWS (outside the katabatic boundary layer). The blue line is the significant fit ($p < 0.01$) for downslope/katabatic winds and the red line is the non-significant fit for upslope winds, while the dashed grey line demarcates no temperature depression.

TCD
9, 2915–2953, 2015

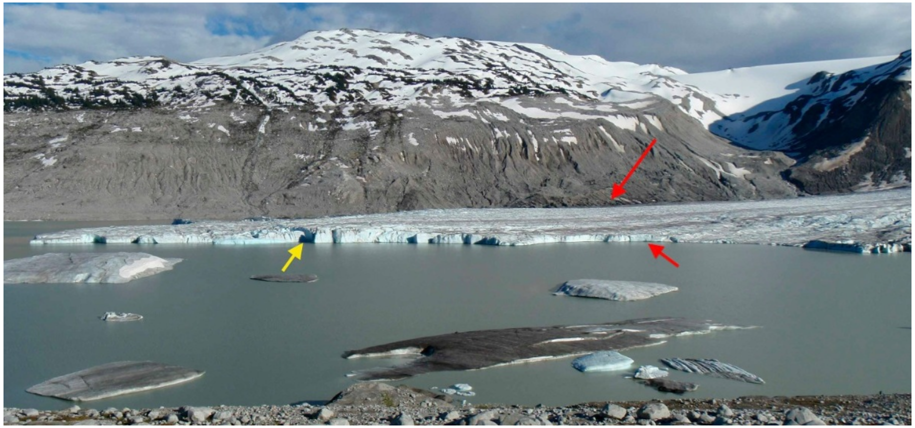

Figure 5. Photograph of Bridge Glacier terminus, 18 June 2013. Note the inflection point (red arrow), which indicates flotation. The yellow arrow indicates a large crevasse that led to calving of a large tabular iceberg from the terminus to the left of arrow.

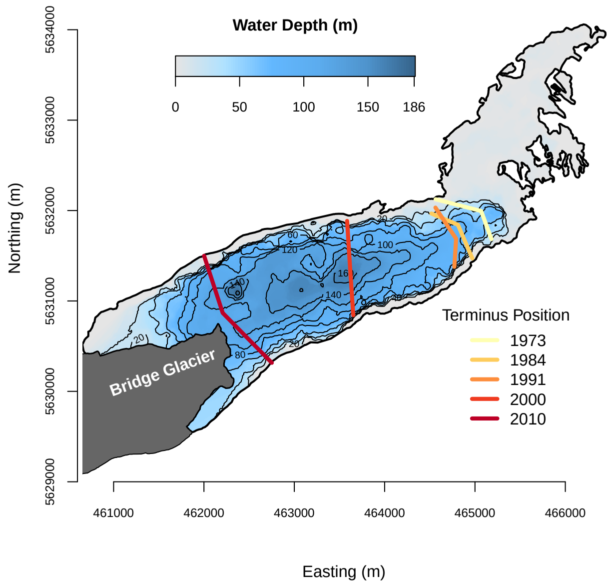

Figure 6. Bathymetry for Bridge Lake, taken over the 2013 field season.

TCD
9, 2915–2953, 2015

The relative contributions of calving and surface ablation

M. Chernos et al.

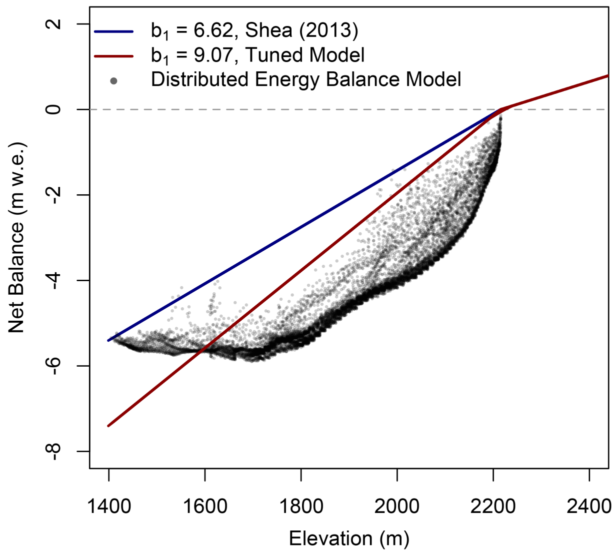

Figure 7. Modelled mass balance gradients from Shea et al. (2013) and a tuned coefficient using distributed energy balance modelling from the 2013 melt season.

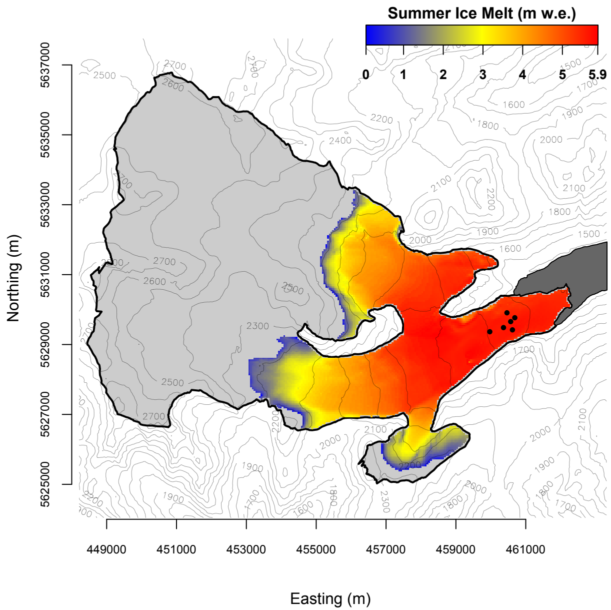

Figure 8. Modelled melt and ablation stakes (black dots) for the study period 20 June to 12 September 2013.

TCD
9, 2915–2953, 2015

The relative contributions of calving and surface ablation

M. Chernos et al.

Title Page
Abstract Introduction
Conclusions References
Tables Figures
Back Close
Full Screen / Esc
Printer-friendly Version
Interactive Discussion

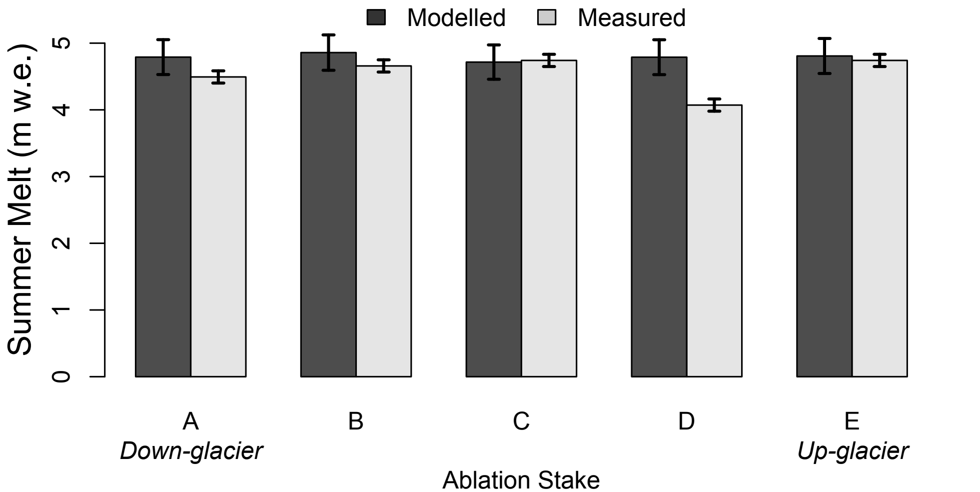

Figure 9. Observed (measured) melt from ablation stakes, and modelled melt from DEBM.

TCD
9, 2915–2953, 2015

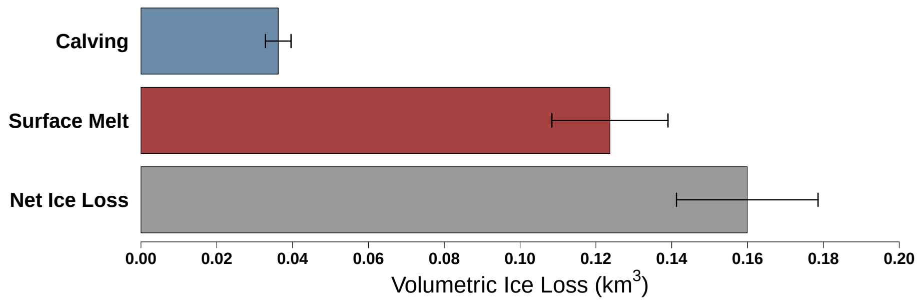

Figure 10. Total volumetric ice loss at Bridge Glacier during the 2013 melt season (ice equivalent).

TCD
9, 2915–2953, 2015

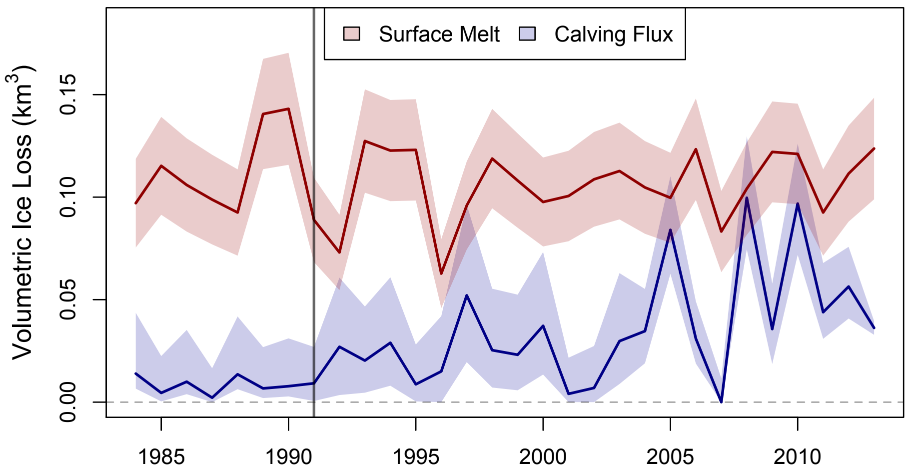

Figure 11. Historical ice loss from calving and surface melt, 1984–2013. Dark vertical line in 1991 indicates period in which terminus reached flotation and calving rates increased.

TCD
9, 2915–2953, 2015

The relative contributions of calving and surface ablation

M. Chernos et al.

Title Page
Abstract Introduction
Conclusions References
Tables Figures
Back Close
Full Screen / Esc
Printer-friendly Version
Interactive Discussion

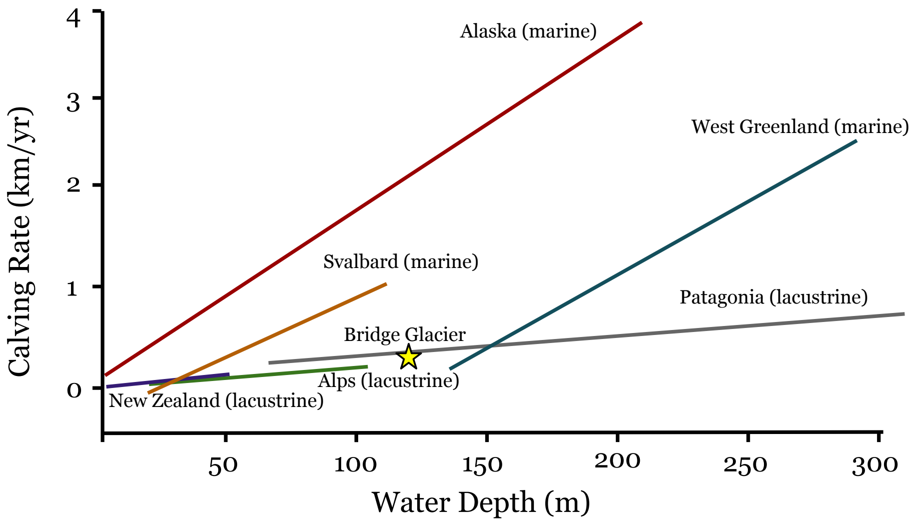

Figure 12. The relationship between calving rate and water depth for freshwater and tidewater glaciers worldwide. Bridge Glacier is denoted by the yellow star. Adapted from Haresign (2004).

TCD
9, 2915–2953, 2015

The relative contributions of calving and surface ablation

M. Chernos et al.